Figure S1

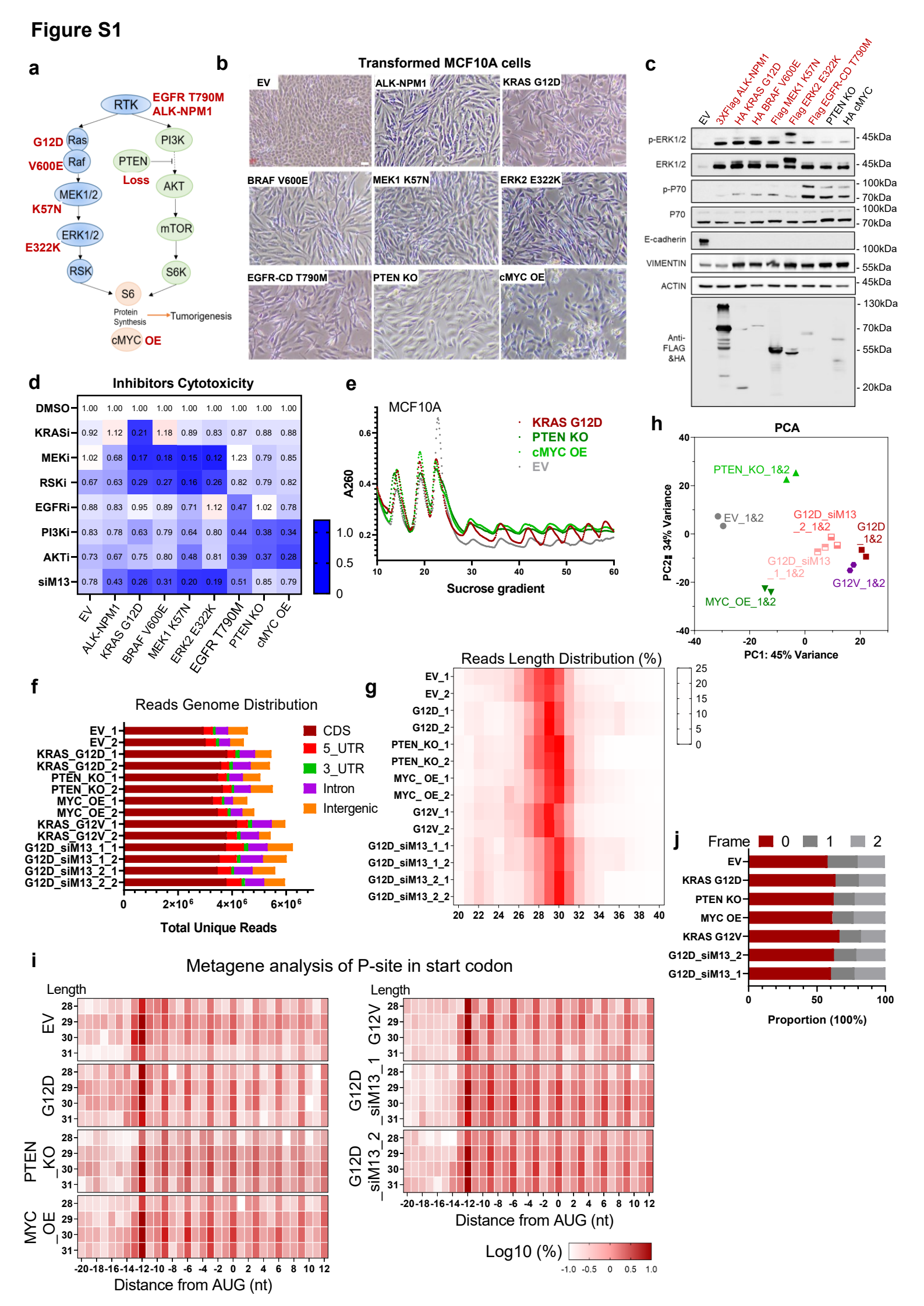
a
RTK
EGFR T790M
ALK-NPM1
G12D
Ras
PI3K
V600E
Raf
PTEN
Loss
AKT
MEK1/2
K57N
ERK1/2
E322K
mTOR
RSK
S6K
S6
Protein Synthesis
Tumorigenesis
cMYC OE
b
Transformed MCF10A cells
EV
ALK-NPM1
KRAS G12D
BRAF V600E
MEK1 K57N
ERK2 E322K
EGFR-CD T790M
PTEN KO
cMYC OE
c
EV
3XFlag ALK-NPM1
HA KRAS G12D
HA BRAF V600E
Flag MEK1 K57N
Flag ERK2 E322K
Flag EGFR-CD T790M
PTEN KO
HA cMYC
p-ERK1/2
ERK1/2
p-P70
P70
E-cadherin
VIMENTIN
ACTIN
Anti-FLAG &HA
45kDa
100kDa
70kDa
55kDa
130kDa
20kDa
d
Inhibitors Cytotoxicity
DMSO
KRASi
MEKi
RSKi
EGFRi
PI3Ki
AKTi
siM13
e
MCF10A
KRAS G12D
PTEN KO
cMYC OE
EV
A260
Sucrose gradient
h
PCA
PTEN_KO_1&2
EV_1&2
G12D_siM13_2_1&2
G12D_1&2
G12D_siM13_1_1&2
G12V_1&2
MYC_OE_1&2
PC2: 34% Variance
PC1: 45% Variance
f
Reads Genome Distribution
EV_1
EV_2
KRAS_G12D_1
KRAS_G12D_2
PTEN_KO_1
PTEN_KO_2
MYC_OE_1
MYC_OE_2
KRAS_G12V_1
KRAS_G12V_2
G12D_siM13_1_1
G12D_siM13_1_2
G12D_siM13_2_1
G12D_siM13_2_2
CDS
5_UTR
3_UTR
Intron
Intergenic
Total Unique Reads
g
Reads Length Distribution (%)
EV_1
EV_2
G12D_1
G12D_2
PTEN_KO_1
PTEN_KO_2
MYC_ OE_1
MYC_ OE_2
G12V_1
G12V_2
G12D_siM13_1_1
G12D_siM13_1_2
G12D_siM13_2_1
G12D_siM13_2_2
j
Frame 0 1 2
EV
KRAS G12D
PTEN KO
MYC OE
KRAS G12V
G12D_siM13_2
G12D_siM13_1
Proportion (100%)
i
Metagene analysis of P-site in start codon
Length
EV
G12D
PTEN KO
MYC OE
G12V
G12D siM13_1
G12D siM13_2
Distance from AUG (nt)
Log10 (%)

Figure S1

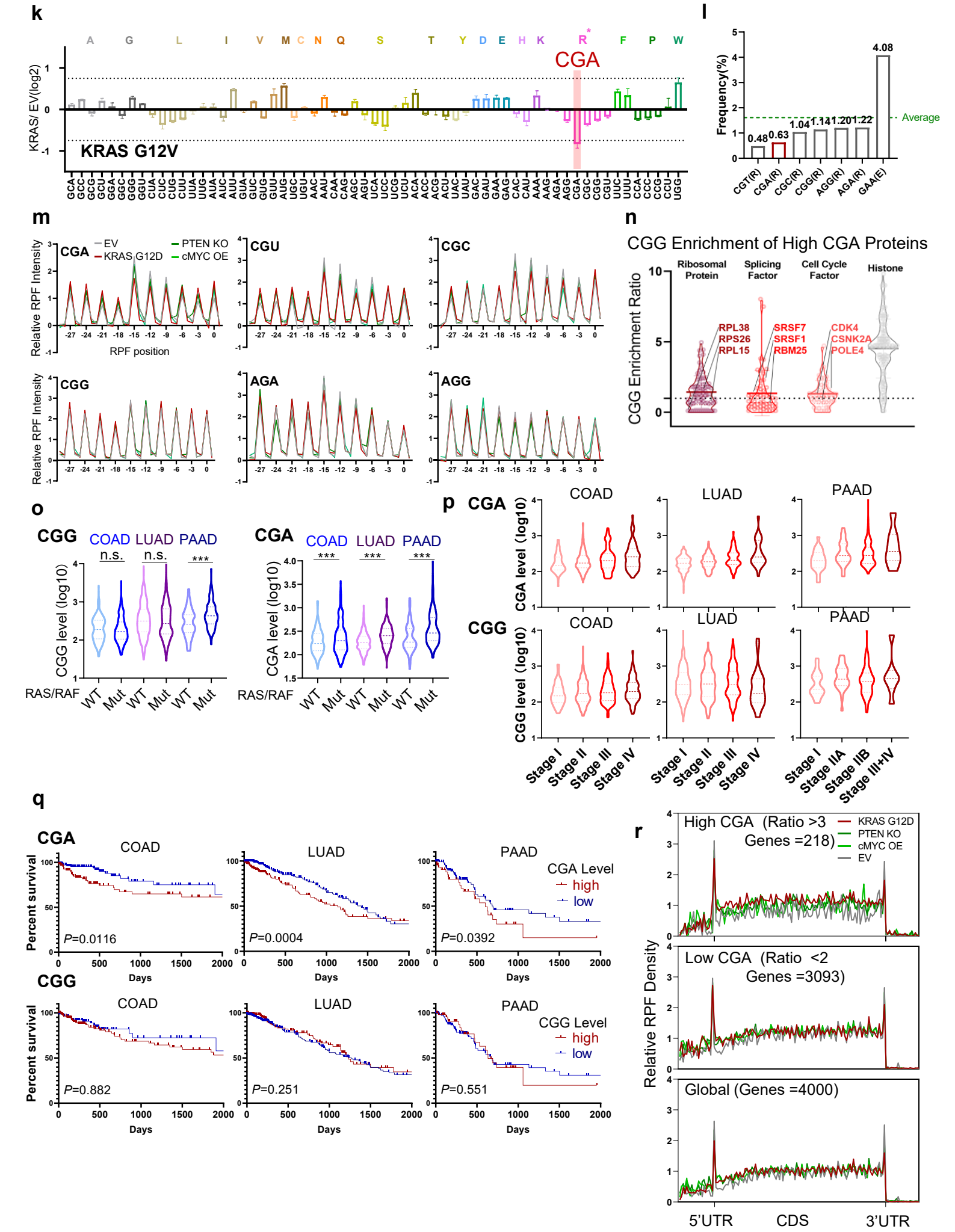
k
KRAS/ EV(log2)
KRAS G12V
CGA
l
Frequency(%)
Average
0.48
0.63
1.04
1.14
1.20
1.22
4.08
CGT(R)
CGA(R)
CGC(R)
CGG(R)
AGG(R)
AGA(R)
GAA(E)
m
CGA
EV
KRAS G12D
PTEN KO
cMYC OE
Relative RPF Intensity
RPF position
CGU
CGC
CGG
AGA
AGG
n
CGG Enrichment of High CGA Proteins
Ribosomal Protein
Splicing Factor
Cell Cycle Factor
Histone
CGG Enrichment Ratio
RPL38
RPS26
RPL15
SRSF7
SRSF1
RBM25
CDK4
CSNK2A
POLE4
o
CGG
COAD LUAD PAAD
n.s.
n.s.
***
CGG level (log10)
RAS/RAF
WT
Mut
CGA
CGA level (log10)
p
CGA
CGG
COAD
LUAD
PAAD
CGA level (log10)
CGG level (log10)
Stage I
Stage II
Stage III
Stage IV
Stage IIA
Stage IIB
Stage III+IV
q
CGA
CGG
COAD
LUAD
PAAD
Percent survival
Days
CGA Level
CGG Level
high
low
P=0.0116
P=0.0004
P=0.0392
P=0.882
P=0.251
P=0.551
r
High CGA (Ratio >3
Genes =218)
Low CGA (Ratio <2
Genes =3093)
Global (Genes =4000)
KRAS G12D
PTEN KO
cMYC OE
EV
Relative RPF Density
5'UTR
CDS
3'UTR

Figure S1

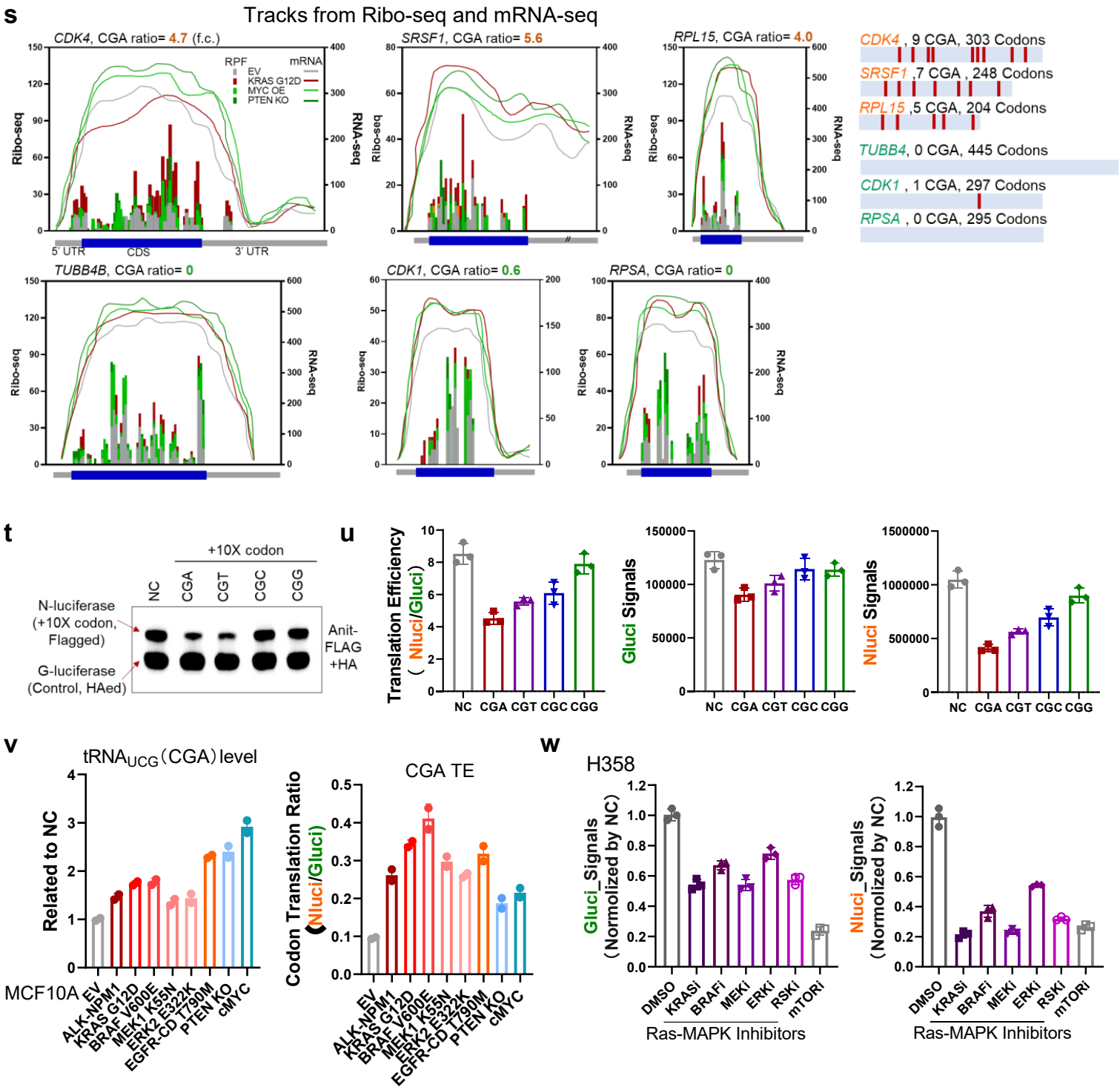
s
Tracks from Ribo-seq and mRNA-seq
CDK4, CGA ratio= 4.7 (f.c.)
SRSF1, CGA ratio= 5.6
RPL15, CGA ratio= 4.0
TUBB4B, CGA ratio= 0
CDK1, CGA ratio= 0.6
RPSA, CGA ratio= 0
RPF
mRNA
EV
KRAS G12D
MYC OE
PTEN KO
Ribo-seq
RNA-seq
5' UTR
CDS
3' UTR
CDK4 , 9 CGA, 303 Codons
SRSF1 ,7 CGA , 248 Codons
RPL15 ,5 CGA, 204 Codons
TUBB4, 0 CGA, 445 Codons
CDK1 , 1 CGA, 297 Codons
RPSA , 0 CGA, 295 Codons
t
+10X codon
NC
CGA
CGT
CGC
CGG
N-luciferase
(+10X codon,
Flagged)
G-luciferase
(Control, HAed)
Anit-
FLAG
+HA
u
Translation Efficiency
(Nluci/Gluci)
Gluci Signals
Nluci Signals
NC CGA CGT CGC CGG
v
tRNAUCG(CGA) level
Related to NC
MCF10A
EV
ALK-NPM1
KRAS G12D
BRAF V600E
MEK1 K55N
ERK2 E322K
EGFR-CD T790M
PTEN KO
cMYC
CGA TE
Codon Translation Ratio
(Nluci/Gluci)
w
H358
Gluci_Signals
(Normolized by NC)
Nluci_Signals
(Normolized by NC)
DMSO
KRASi
BRAFi
MEKi
ERKi
RSKi
mTORi
Ras-MAPK Inhibitors

Supplementary Fig. S1. a, Schematic of oncogenic drivers transfected in MCF10A cells (highlighted in red). Left: classical RAS-MAPK pathway (blue), right: PI3K-mTOR pathway (green). **b**, Morphological images of transformed MCF10A cells. MCF10A^{EV} retained epithelial-like while other cells showed tumor-like morphology. **c**, Immunoblot analysis of the indicated MCF10A cells. pERK as a marker of RAS pathway activation, pP70 as a marker of mTOR pathway activation, E-cadherin as a marker of normal cell, and VIMENTIN as a marker of transformed cell. **d**, Cell viability assay of the indicated MCF10A cells treated with RAS-MAPK pathway inhibitors for 8 days (KRASi: AMG510, 1μM; MEKi: Trametinib, 0.5μM; RSKi: BI-D1870, 1μM; EGFRi: Oritinib, 1μM; PI3Ki: Omipalisib, 0.5μM; AKTi: MK-2206, 1μM). **e**, Polysome profiling of the indicated MCF10A cells. EV cell showed more mono-somes and fewer polysomes compared to other three transformed cells. **f**, Genomic distribution of Ribo-seq reads. Percentage of uniquely mapped reads distributed across CDS, 5' UTR, 3' UTR, intronic, and intergenic regions. Sequencing depth was normalized to total uniquely mapped reads within the protein-coding transcriptome (CDS + UTRs). **g**, Length distribution of uniquely mapped ribosome-protected fragments (RPFs). Read lengths predominantly range from 27 to 31 nucleotides (nt), consistent with the characteristic size of RPFs in mammalian cells. **h**, Principal component analysis (PCA) of Ribo-seq samples. Biological replicates from each experimental group cluster closely, demonstrating high reproducibility across the datasets. **i**, Metagene analysis of P-site offsets at the start codon. Cumulative distribution of RPFs (28–31 nt) relative to the start codon (AUG). A prominent peak at -12 nt identifies the P-site offset, corresponding to an A-site offset at -15 nt. The observed 3-nt periodicity reflects synchronous ribosome translocation along the mRNA. **j**, Distribution of RPFs across reading frames. Proportion of RPFs mapped to the three possible reading frames. Over 50% map to Frame 0, confirming high-quality, codon-resolution mapping without significant frame shifts. **k**, Codon occupancy shifts in MCF10A$^{KRAS\ G12V}$ cells compared to empty vector (EV) control cells. **l**, Frequency of the 6 arginine codons across the human genomic coding sequence (hg38). **m**, RPF distribution across arginine codons in the indicated MCF10A cells. *KRAS*^{G12D} cells showed increased TE at CGA, CGU, and CGC codons compared to other lines, with no significant change at other arginine codons. As a control of Fig. 1c. **n**, CGG enrichment ratio of high-CGA protein groups. Histone proteins, used as a control, were enriched for CGG codons. As control of Fig. 1f. **o**, CGA and CGG codon usage levels in patients with or without RAS/RAF activation in colon (COAD), lung (LUAD), and pancreatic (PAAD) adenocarcinomas from the TCGA database. CGA codon level data were obtained from the TRIC database. Data are presented as mean ± SD, analyzed by paired t-test (***$P < 0.001$). **p**, CGA and CGG levels of COAD, LUAD and PAAD patients grouped by different tumor stages. More malignant tumors had a higher CGA level, but not in CGG. **q**, Kaplan-Meier survival analysis of patients stratified by high or low CGA or CGG codon usage levels in COAD, LUAD, and PAAD (the same datasets as in S1o). Statistical significance was determined by the log-rank test. **r**, Metagene analysis of the indicated MCF10A cells across high-CGA (ratio >3, n=218), low-CGA (ratio <2, n=3093) and global genes (n=4000, FPKM >10). High-CGA genes showed elevated translation in *KRAS*^{G12D} cells. **s**, Transcriptome (RNA-seq) and translatome (Ribo-seq) read tracks for high-CGA genes (*CDK4, SRSF1, RPL15*) and low-CGA control genes (*TUBB4B, CDK1, RPSA*) across the indicated MCF10A cells. High-CGA genes exhibited elevated translation under similar transcript levels in *KRAS*^{G12D} cells (left). Schematic of CGA codon in those 6 genes, CGA highlighted in red (right). **t**, Immunoblotting of the dual-tag reporter. HA-tagged G-luciferase (control) and Flag-tagged N-luciferase (reporter) signals were detected concurrently; the Flag/HA signal ratio reflects TE. Note the marked reduction of

CGA- and CGT-reporter levels relative to the internal control. For the negative control (NC), the 10× tandem codon cassette was replaced with a 2× GSSSG linker sequence. **u**, Quantitative analysis of TE. Rare codons (CGA and CGT) exhibit significantly lower translational output relative to the synonymous optimal CGG codon in HEK293T cells. **v**, Non-normalized CGA TE and $tRNA_{UCG}$ abundance of the indicated MCF10A cells. Related to Fig. 1j. **w**, Raw dual-luciferase signals from CGA TE reporter assays in H358 cells. Related to Fig. 1k.

Figure S2

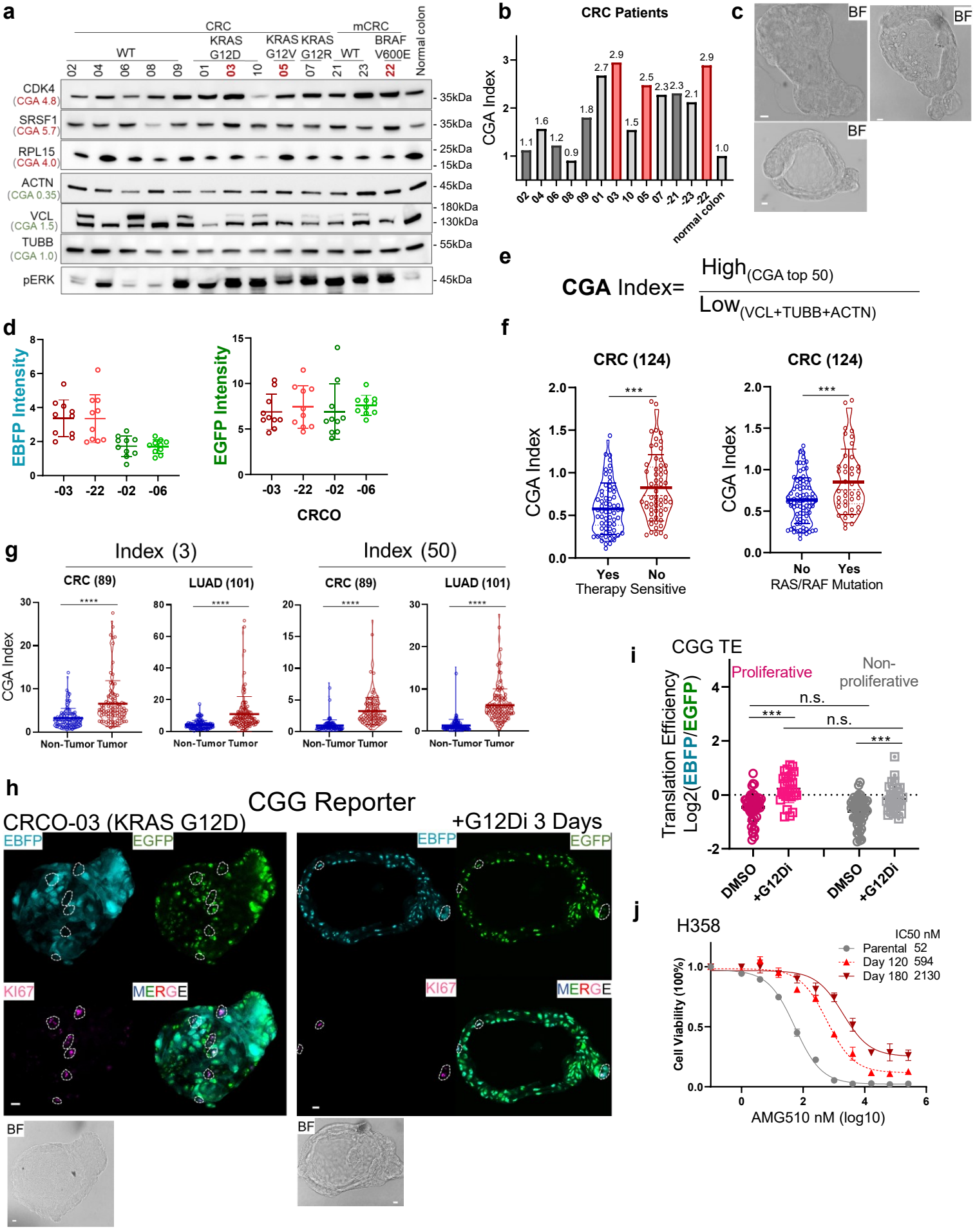
a
CRC
mCRC
WT
KRAS G12D
KRAS G12V
KRAS G12R
WT
BRAF V600E
Normal colon
02 04 06 08 09 01 03 10 05 07 21 23 22
CDK4 (CGA 4.8)
SRSF1 (CGA 5.7)
RPL15 (CGA 4.0)
ACTN (CGA 0.35)
VCL (CGA 1.5)
TUBB (CGA 1.0)
pERK
35kDa
35kDa
25kDa
15kDa
45kDa
180kDa
130kDa
55kDa
45kDa
b
CRC Patients
CGA Index
1.1 1.6 1.2 0.9 1.8 2.7 2.9 1.5 2.5 2.3 2.3 2.1 2.9 1.0
02 04 06 08 09 01 03 10 05 07 21 23 22 normal colon
c
BF
BF
BF
d
EBFP Intensity
EGFP Intensity
-03 -22 -02 -06
CRCO
e
CGA Index= High(CGA top 50) / Low(VCL+TUBB+ACTN)
f
CRC (124)
CRC (124)
CGA Index
***
Yes No
Therapy Sensitive
No Yes
RAS/RAF Mutation
g
Index (3)
Index (50)
CRC (89)
LUAD (101)
CRC (89)
LUAD (101)
CGA Index
****
Non-Tumor Tumor
i
CGG TE
Proliferative
Non-proliferative
Translation Efficiency Log2(EBFP/EGFP)
n.s.
***
n.s.
***
DMSO +G12Di DMSO +G12Di
h
CGG Reporter
CRCO-03 (KRAS G12D)
+G12Di 3 Days
EBFP
EGFP
KI67
MERGE
BF
j
H358
IC50 nM
Parental 52
Day 120 594
Day 180 2130
Cell Viability (100%)
AMG510 nM (log10)

Supplementary Fig. S2. a, Immunoblot analysis of the indicated proteins from CRC patient tissues. CGA enrichment ratios are indicated below each protein symbol. **b**, CGA index of the CRC patients determined by the formula shown in Fig. 2a. Patients with tumor recurrence are highlighted in red. **c**, Bright field images of CRC PDOs shown in Fig. 2e and 2j. Scale bars: 20μm. **d**, Raw fluorescence intensities of EGFP and EBFP from the codon TE reporter assay. Related to Fig. 2d. **e**, Formula illustrating the CGA index calculated from the top 50 CGA-enriched proteins. **f**, Re-analysis of the data shown in Fig. 2g and 2h using the CGA index based on the top 50 proteins, confirming the original trends with improved statistical significance. **g**, CGA index of CRC and LUAD patients grouped by tumor or non-tumor tissues. Dataset was analyzed from Xu et al., 2020 (LUAD) and Vasaikar et al., 2019 (CRC). The CGA index in left panel was calculated by 3 genes and the right was calculated by top 50 genes. Data are presented as mean± SD. **h**, IF analysis of EBFP, EGFP and Ki67 in CRCO-03 PDOs expressing the CGG TE reporter, as control of Fig. 2j. The CGG TE was not elevated in proliferative cells. Scale bars: 20μm. **i**, Quantification of CGG TE in CRCO-03. **j**, Cell viability curves of the parental and resistant H358 cells under AMG510 treatment (n=3). Data are presented as mean ± SEM. Related to Fig. 2m. Data from this Figure were analyzed by two-tailed unpaired t-test (*P < 0.05, **P < 0.01, ***P < 0.001).

Figure S3

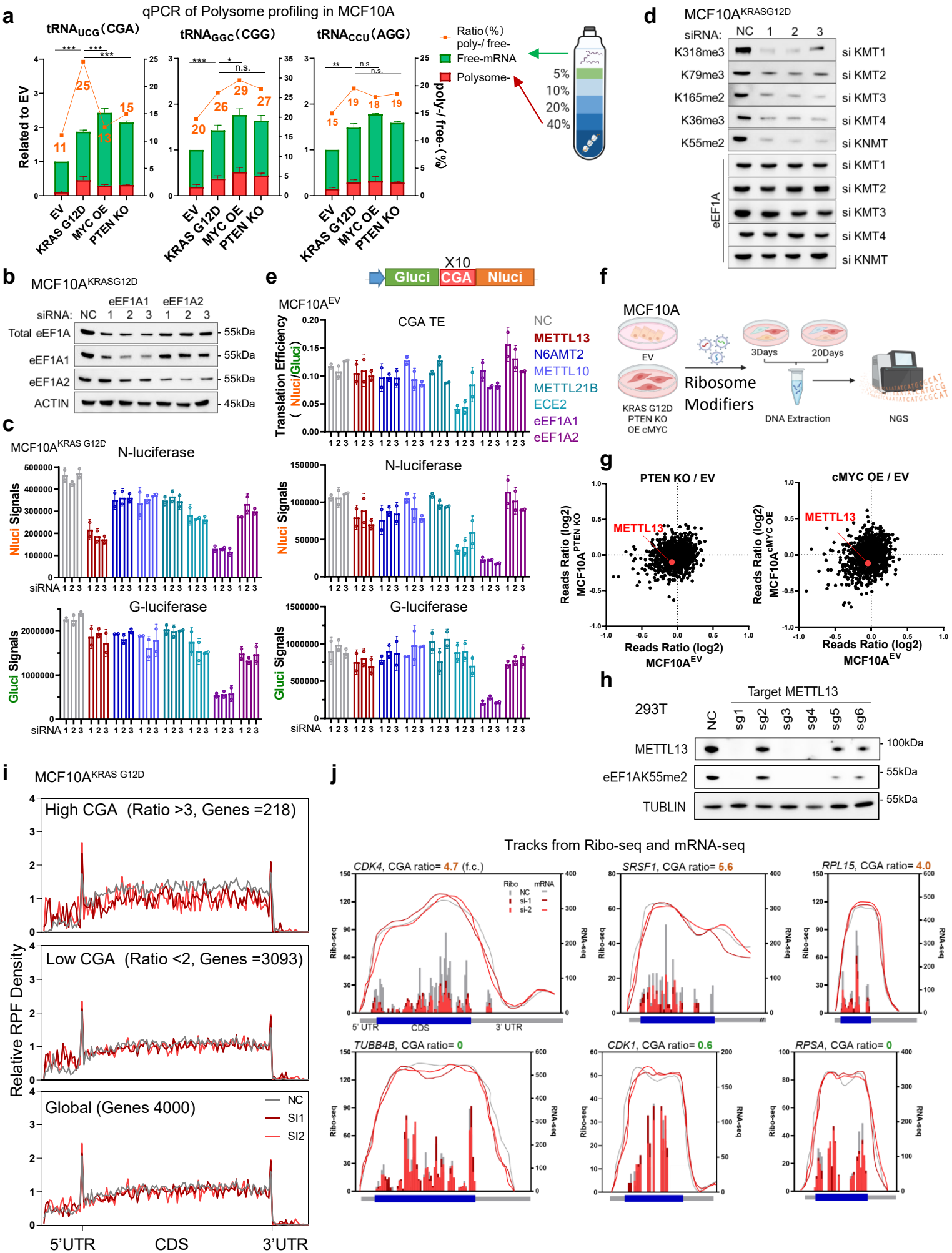
a
qPCR of Polysome profiling in MCF10A
tRNA_UCG(CGA)
tRNA_GGC(CGG)
tRNA_CCU(AGG)
Related to EV
poly-/ free-(%)
Ratio(%) poly-/ free-
Free-mRNA
Polysome-
5%
10%
20%
40%
EV
KRAS G12D
MYC OE
PTEN KO
b
MCF10A^KRASG12D
siRNA: NC 1 2 3 1 2 3
eEF1A1
eEF1A2
Total eEF1A
eEF1A1
eEF1A2
ACTIN
55kDa
45kDa
c
MCF10A^KRAS G12D
N-luciferase
G-luciferase
Nluci Signals
Gluci Signals
siRNA
e
X10
Gluci
CGA
Nluci
MCF10A^EV
CGA TE
Translation Efficiency (Nluci/Gluci)
NC
METTL13
N6AMT2
METTL10
METTL21B
ECE2
eEF1A1
eEF1A2
f
MCF10A
EV
KRAS G12D
PTEN KO
OE cMYC
Ribosome Modifiers
3Days
20Days
DNA Extraction
NGS
g
PTEN KO / EV
cMYC OE / EV
METTL13
Reads Ratio (log2) MCF10A^PTEN KO
Reads Ratio (log2) MCF10A^cMYC OE
Reads Ratio (log2) MCF10A^EV
d
MCF10A^KRASG12D
siRNA: NC 1 2 3
K318me3
K79me3
K165me2
K36me3
K55me2
eEF1A
si KMT1
si KMT2
si KMT3
si KMT4
si KNMT
h
293T
Target METTL13
NC
sg1
sg2
sg3
sg4
sg5
sg6
METTL13
eEF1AK55me2
TUBLIN
100kDa
55kDa
i
MCF10A^KRAS G12D
High CGA (Ratio >3, Genes =218)
Low CGA (Ratio <2, Genes =3093)
Global (Genes 4000)
NC
SI1
SI2
Relative RPF Density
5'UTR
CDS
3'UTR
j
Tracks from Ribo-seq and mRNA-seq
CDK4, CGA ratio= 4.7 (f.c.)
SRSF1, CGA ratio= 5.6
RPL15, CGA ratio= 4.0
TUBB4B, CGA ratio= 0
CDK1, CGA ratio= 0.6
RPSA, CGA ratio= 0
Ribo
mRNA
Ribo-seq
RNA-seq
5' UTR
CDS
3' UTR

Figure S3

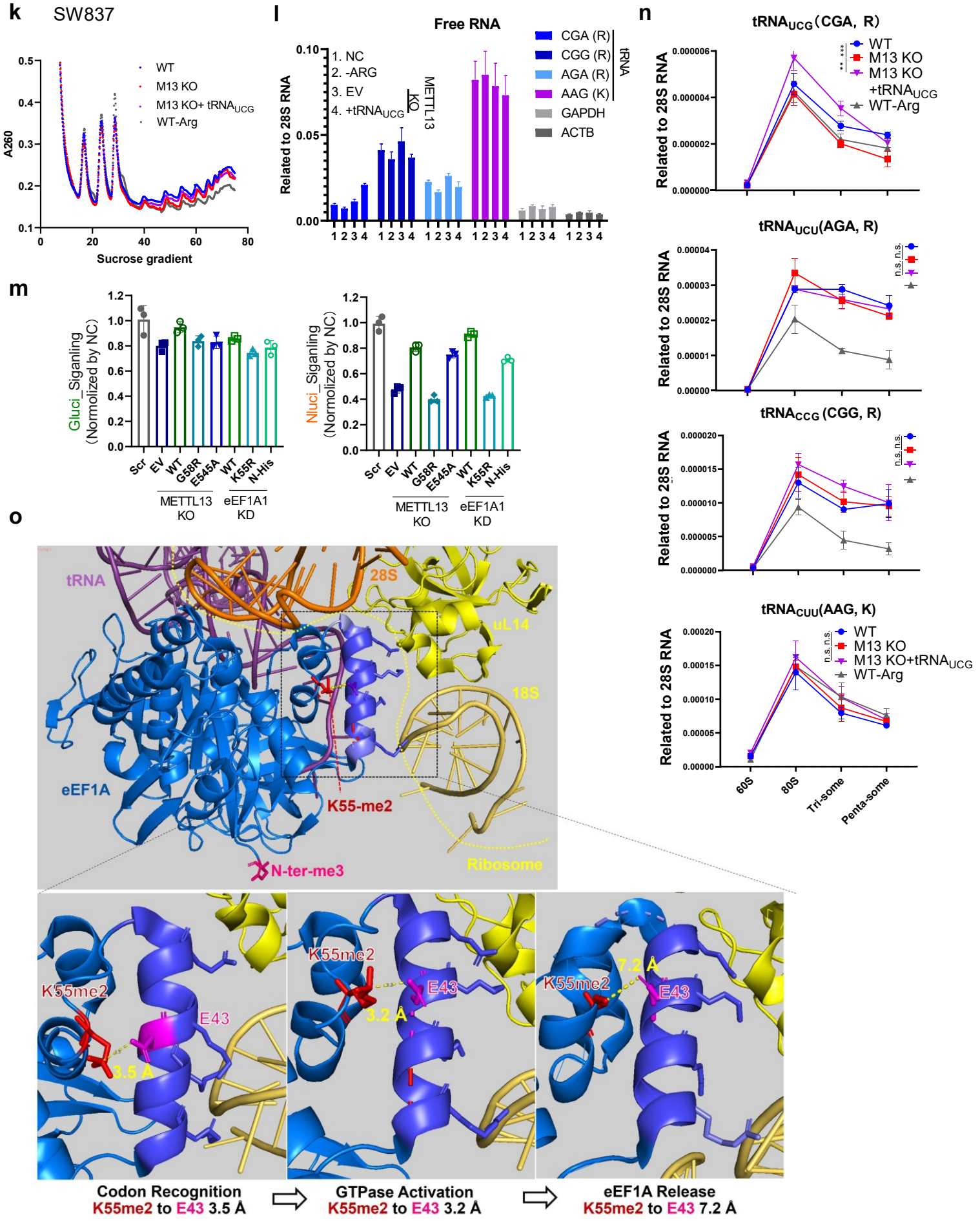
k
SW837
WT
M13 KO
M13 KO+ tRNAUCG
WT-Arg
A260
Sucrose gradient
l
Free RNA
1. NC
2. -ARG
3. EV
4. +tRNAUCG
METTL13 KO
CGA (R)
CGG (R)
AGA (R)
AAG (K)
tRNA
GAPDH
ACTB
Related to 28S RNA
n
tRNAUCG(CGA, R)
M13 KO +tRNAUCG
tRNAUCU(AGA, R)
tRNACCG (CGG, R)
tRNACUU(AAG, K)
M13 KO+tRNAUCG
n.s.
60S
80S
Tri-some
Penta-some
m
Gluci_Siganling (Normolized by NC)
Nluci_Siganling (Normolized by NC)
Scr
EV
WT
G58R
E545A
K55R
N-His
METTL13 KO
eEF1A1 KD
o
tRNA
28S
uL14
18S
eEF1A
K55-me2
N-ter-me3
Ribosome
K55me2
E43
3.5 Å
3.2 Å
7.2 Å
Codon Recognition
K55me2 to E43 3.5 Å
GTPase Activation
K55me2 to E43 3.2 Å
eEF1A Release
K55me2 to E43 7.2 Å

Supplementary Fig. S3. a, Ratio of polysome bound tRNA (CGA, CGG and AGG) in the indicated MCF10A cells. Green columns are the abundance of free-tRNA, red columns are the abundance of polysome-bound-tRNA, orange dots are ratio of polysome-/ free- tRNA. **b**, Knockdown of eEF1A1 and eEF1A2 in MCF10A$^{KRAS\ G12D}$ cells. **c**, Translation control (Gluci signals) and CGA TE (Nluci /Gluci signals) from CGA TE reporter assays in MCF10A$^{KRAS\ G12D}$ cells. Related to Fig. 3b. **d**, Immunoblot analysis of eEF1A methylations in MCF10A$^{KRAS\ G12D}$ cells with the knockdown of the corresponding methyltransferases. siRNAs were transfected twice in 6 Days. Related to Fig. 3b. **e**, CGA TE alteration upon knockdown of eEF1A and its methyltransferases in MCF10A^{EV} cells. As control of Fig. 3b. **f**, Schematic of the cell growth-based CRISPR-Cas9 screen in the indicated MCF10A cells. **g**, CRISPR-Cas9 screen in MCF10A$^{PTEN\ KO}$ and MCF10A$^{MYC\ OE}$ cells. METTL13 is highlighted. As control of Fig. 3c. **h**, Immunoblotting analysis of METTL13 knockout efficiency using six distinct sgRNAs in HEK293T cells. sgRNAs 2, 5, and 6 showed suboptimal knockout efficiency. Related to Fig. 3c. **i**, Metagene analysis of MCF10A$^{KRAS\ G12D}$ cells in the control (NC) and METTL13 KD conditions. High-CGA genes showed decreased translation upon METTL13 KD. **j**, Transcriptome (RNA-seq) and translatome (Ribo-seq) read tracks for high-CGA genes (*CDK4, SRSF1, RPL15*) and low-CGA control genes (*TUBB4B, CDK1, RPSA*) in MCF10A$^{KRAS\ G12D}$ cells with METTL13 KD. Compared to NC, METTL13 KD cells showed decreased translation of high-CGA genes at similar transcript levels. **k**, Polysome profiling in the indicated SW837 cells. WT-Arg means Arginine deprivation, as a positive control. Related to Fig. 3g. **l**,**m**, Abundances of the free tRNA (l) and ribosome bound tRNA (m) detected by qPCR in the indicated SW837 cells. Related to Fig. 3g. **n**, Raw dual-luciferase signals in SW837 cells related to Fig. 3i. **o**, Structure of eEF1A during codon recognition process. eEF1A: dark blue, uL14 (RPL23): yellow, 28S RNA: orange, 18S RNA: yellow, tRNA: violet. There is a hydrogen bond between K55 and E43 residues of eEF1A (highlighted by red).

Figure S4

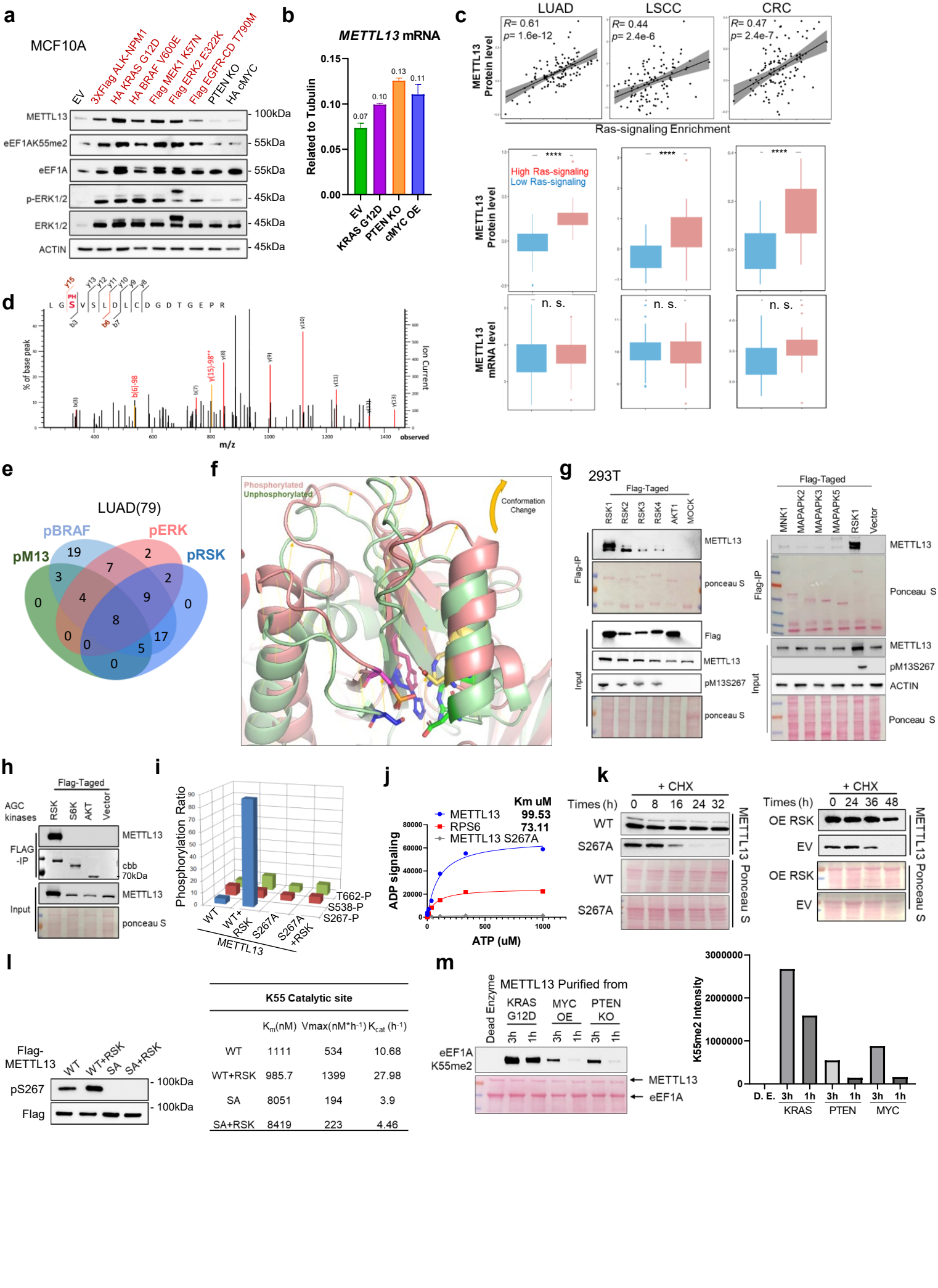
a
MCF10A
EV
3XFlag ALK-NPM1
HA KRAS G12D
HA BRAF V600E
Flag MEK1 K57N
Flag ERK2 E322K
Flag EGFR-CD T790M
PTEN KO
HA cMYC
METTL13
eEF1AK55me2
eEF1A
p-ERK1/2
ERK1/2
ACTIN
100kDa
55kDa
55kDa
45kDa
45kDa
45kDa
b
METTL13 mRNA
Related to Tubulin
0.15
0.10
0.05
0.00
0.07
0.10
0.13
0.11
EV
KRAS G12D
PTEN KO
cMYC OE
c
LUAD
LSCC
CRC
R= 0.61
p= 1.6e-12
R= 0.44
p= 2.4e-6
R= 0.47
p= 2.4e-7
METTL13 Protein level
Ras-signaling Enrichment
High Ras-signaling
Low Ras-signaling
****
METTL13 mRNA level
n. s.
d
L G S V S L D L C D G D T G E P R
% of base peak
Ion Current
m/z
observed
b(6)-98
y(15)-98**
e
LUAD(79)
pBRAF
pERK
pM13
pRSK
19
2
7
3
2
4
9
0
0
8
0
17
0
5
0
f
Phosphorylated
Unphosphorylated
Conformation Change
g
293T
Flag-Taged
RSK1
RSK2
RSK3
RSK4
AKT1
MOCK
MNK1
MAPAPK2
MAPAPK3
MAPAPK5
Vector
Flag-IP
Input
METTL13
ponceau S
Flag
pM13S267
ACTIN
h
Flag-Taged
AGC kinases
RSK
S6K
AKT
Vector
FLAG -IP
cbb 70kDa
i
Phosphorylation Ratio
T662-P
S538-P
S267-P
WT
WT+ RSK
S267A
S267A +RSK
METTL13
j
Km uM
METTL13 99.53
RPS6 73.11
METTL13 S267A
ADP signaling
ATP (uM)
k
+ CHX
Times (h)
0 8 16 24 32
0 24 36 48
WT
S267A
OE RSK
EV
METTL13 Ponceau S
l
Flag-METTL13
WT
WT+RSK
SA
SA+RSK
pS267
Flag
100kDa
100kDa
K55 Catalytic site
Km(nM) Vmax(nM*h-1) Kcat (h-1)
WT 1111 534 10.68
WT+RSK 985.7 1399 27.98
SA 8051 194 3.9
SA+RSK 8419 223 4.46
m
METTL13 Purified from
Dead Enzyme
KRAS G12D
MYC OE
PTEN KO
3h
1h
eEF1A K55me2
METTL13
eEF1A
K55me2 Intensity
3000000
2000000
1000000
0
D. E.
KRAS
PTEN
MYC

Figure S4

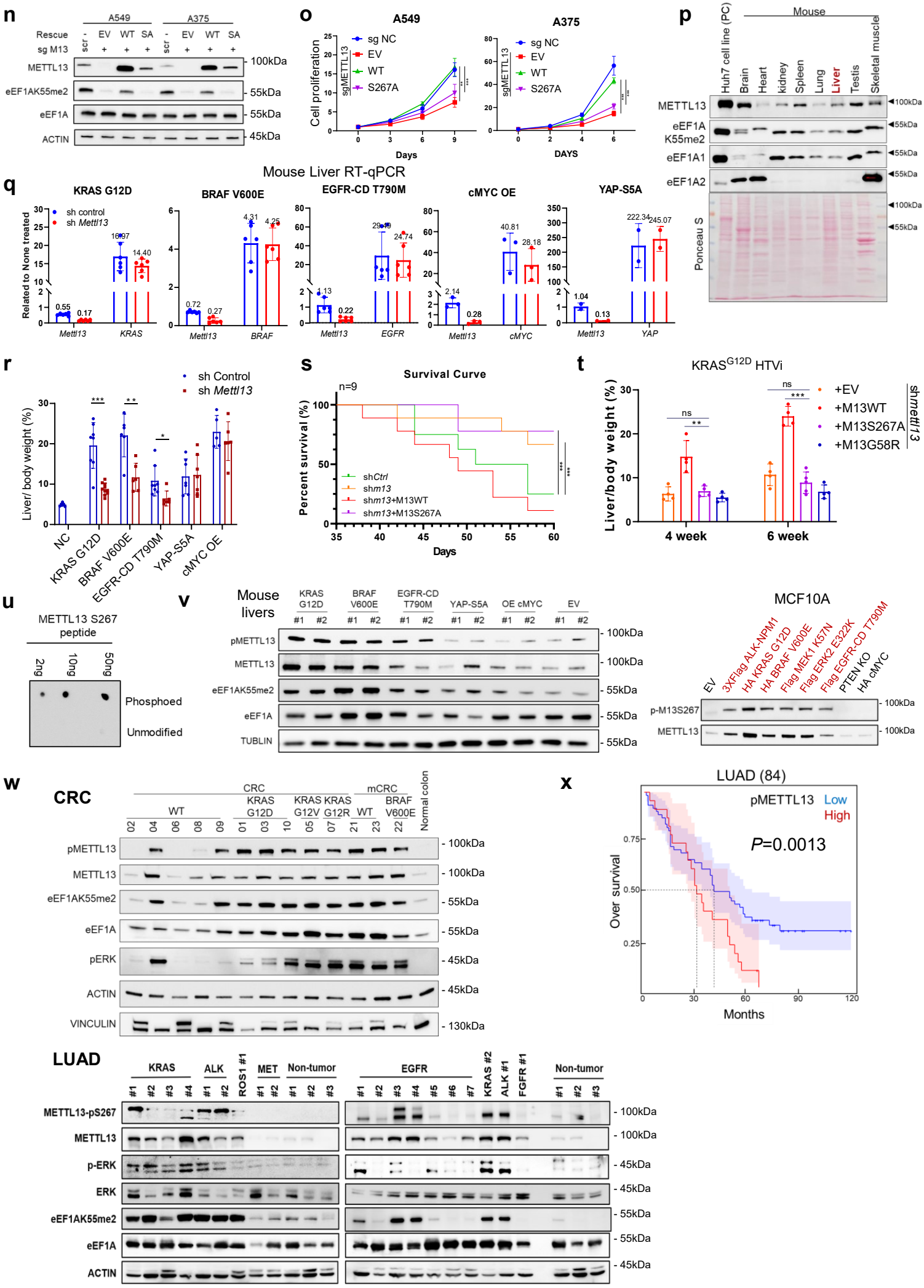
n
A549
A375
Rescue
sg M13
METTL13
eEF1AK55me2
eEF1A
ACTIN
100kDa
55kDa
45kDa
o
A549
A375
sg NC
EV
WT
S267A
Cell proliferation
Days
DAYS
p
Mouse
Huh7 cell line (PC)
Brain
Heart
kidney
Spleen
Lung
Liver
Testis
Skeletal muscle
eEF1A1
eEF1A2
Ponceau S
q
Mouse Liver RT-qPCR
KRAS G12D
BRAF V600E
EGFR-CD T790M
cMYC OE
YAP-S5A
sh control
sh Mettl13
Related to None treated
Mettl13
KRAS
BRAF
EGFR
cMYC
YAP
r
sh Control
sh Mettl13
Liver/ body weight (%)
NC
KRAS G12D
BRAF V600E
EGFR-CD T790M
YAP-S5A
cMYC OE
s
Survival Curve
n=9
Percent survival (%)
Days
shCtrl
shm13
shm13+M13WT
shm13+M13S267A
t
KRASG12D HTVi
Liver/body weight (%)
4 week
6 week
+EV
+M13WT
+M13S267A
+M13G58R
shmettl13
u
METTL13 S267 peptide
2ng
10ng
50ng
Phosphoed
Unmodified
v
Mouse livers
KRAS G12D
BRAF V600E
EGFR-CD T790M
YAP-S5A
OE cMYC
EV
pMETTL13
METTL13
eEF1AK55me2
eEF1A
TUBLIN
MCF10A
EV
3XFlag ALK-NPM1
HA KRAS G12D
HA BRAF V600E
Flag MEK1 K57N
Flag ERK2 E322K
Flag EGFR-CD T790M
PTEN KO
HA cMYC
p-M13S267
METTL13
w
CRC
WT
KRAS G12D
KRAS G12V
KRAS G12R
mCRC
BRAF V600E
Normal colon
pMETTL13
METTL13
eEF1AK55me2
eEF1A
pERK
ACTIN
VINCULIN
LUAD
KRAS
ALK
ROS1 #1
MET
Non-tumor
EGFR
KRAS #2
ALK #1
FGFR #1
Non-tumor
METTL13-pS267
METTL13
p-ERK
ERK
eEF1AK55me2
eEF1A
ACTIN
x
LUAD (84)
pMETTL13 Low
High
P=0.0013
Over survival
Months

Supplementary Fig. S4. a, Immunoblot analyses of METTL13 and eEF1A K55me2 levels in the indicated MCF10A cells. **b**, RT-qPCR of *METTL13* mRNA levels in the indicated MCF10A cells. METTL13 expression was not significantly altered in $KRAS^{G12D}$ cells compared to EV. Related to Fig. 4a. **c**, (Top) Pearson correlation analysis between the protein level of METTL13 and RAS pathway activation in LUAD, LSCC, and CRC cohorts from TCGA database, (bottom) METTL13 protein level upregulated in RAS-MAPK activated patients but not mRNA level. Data are presented as mean ± SD, analyzed by paired t-test (***P* < 0.01, ****P* < 0.001). **d**, Mass spectrometry identification of METTL13 phosphorylation at S267. METTL13 was excised from a Phos-tag gel band corresponding to the phosphorylated form. Related to Fig. 4a. **e**, Overlap between the phosphoproteins of the RAS-MAPK pathway and pS267-METTL13 from LUAD patient phosphoproteomics dataset. **f**, Structural comparison of METTL13 with (Pink) and without (Green) S267 phosphorylation predicted by AlphaFold3. Yellow lines indicate conformational changes. **g**, **h**, Co-IP of overexpressed Flag-tagged MAPKAPK (g) and AGC (h) kinases with endogenous METTL13 in HEK293T cells. METTL13 specifically interacted with RSKs, especially the RSK1. **i**, *In vitro* kinase assay of RSK-mediated METTL13 phosphorylation at S267 and detection by LC-MS. **j**, *In vitro* kinase assay of RSK activity toward METTL13 and RPS6, quantified by ADP luminescence. The kinetic parameters were derived by fitting the data to the Michaelis-Menten equation. **k**, (Left) Half-life assay of METTL13 wild-type versus the S267A phosphodeficient mutant. (Right) Half-life assay of METTL13 with versus without RSK overexpression. **l**, (Left) Immunoblot of METTL13 phosphorylation from the kinase assay in Fig. 4f. (Right) Michaelis-Menten kinetic constants derived from the data in Fig. 4f. **m**, *In vitro* methyltransferase activity assay of METTL13 toward eEF1A K55. METTL13 was purified from $KRAS^{G12D}$, *MYC*-OE, or *PTEN*-KO transformed MCF10A cells. **n**, Immunoblot analyses of METTL13 and eEF1A K55me2 levels in the indicated A549 ($KRAS^{G12S}$) and A375 ($BRAF^{V600E}$) cells. **o**, Cell proliferation assay of A549 and A375 cells. METTL13 wild-type rescued the growth defect caused by METTL13 KO, while not the S267A mutant. **p**, Immunoblot analysis of METTL13, eEF1A and eEF1A K55me2 levels in various mouse organs. Liver shows a low METTL13 expression. **q**, **r**, RT-qPCR confirming knockdown of endogenous *Mettl13* and overexpression of onco-drivers in mouse livers (q), Liver/body weight ratio (r) of HTVi mouse models (n = 3–6), related to Fig. 4h. Data are presented as mean ± SD, analyzed by paired t-test (**P*<0.05, ***P* < 0.01, ****P* < 0.001). **s**, **t**, Survival curve (s, n=9) and liver/body weight ratio (t, n=4) of HTVi mouse models, related to Fig. 4i. Statistical significance was determined by the log-rank test. **u**, Dot blot verification of the pS267-METTL13 specific antibody. Antibody is diluted in 1:5000. **v**, Immunoblotting analysis of indicated proteins in mouse liver from HTVi models (left) and MCF10A cells (right). **w**, Immunoblotting analysis of METTL13, pS267-METTL13 and eEF1A K55me2 levels in LUAD and CRC patient tissues with the indicated mutations. mCRC: metastatic colorectal cancer. Related to Fig. 4k. **x**, Kaplan-Meier survival analysis of LUAD cohort stratified by the level of pS267-METTL13 (Low =61, High= 23). Log-rank test.

Figure S5

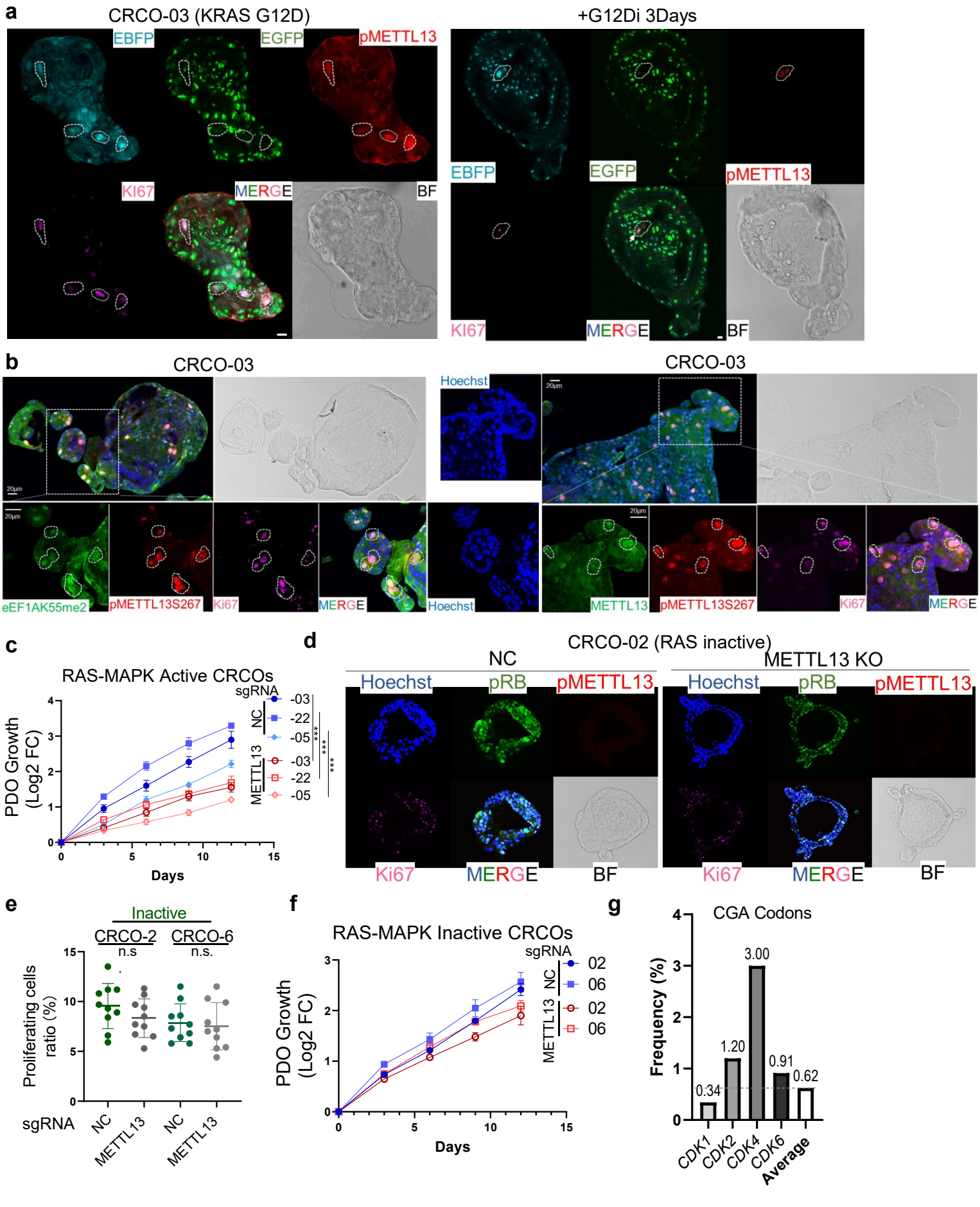
a
CRCO-03 (KRAS G12D)
+G12Di 3Days
EBFP
EGFP
pMETTL13
KI67
MERGE
BF
b
CRCO-03
CRCO-03
Hoechst
eEF1AK55me2
pMETTL13S267
Ki67
METTL13
c
RAS-MAPK Active CRCOs
PDO Growth (Log2 FC)
Days
sgRNA
NC
METTL13
-03
-22
-05
d
CRCO-02 (RAS inactive)
NC
METTL13 KO
Hoechst
pRB
pMETTL13
Ki67
MERGE
BF
e
Inactive
CRCO-2
CRCO-6
n.s
Proliferating cells ratio (%)
sgRNA
f
RAS-MAPK Inactive CRCOs
PDO Growth (Log2 FC)
Days
02
06
g
CGA Codons
Frequency (%)
3.00
1.20
0.91
0.62
0.34
CDK1
CDK2
CDK4
CDK6
Average

Figure S5

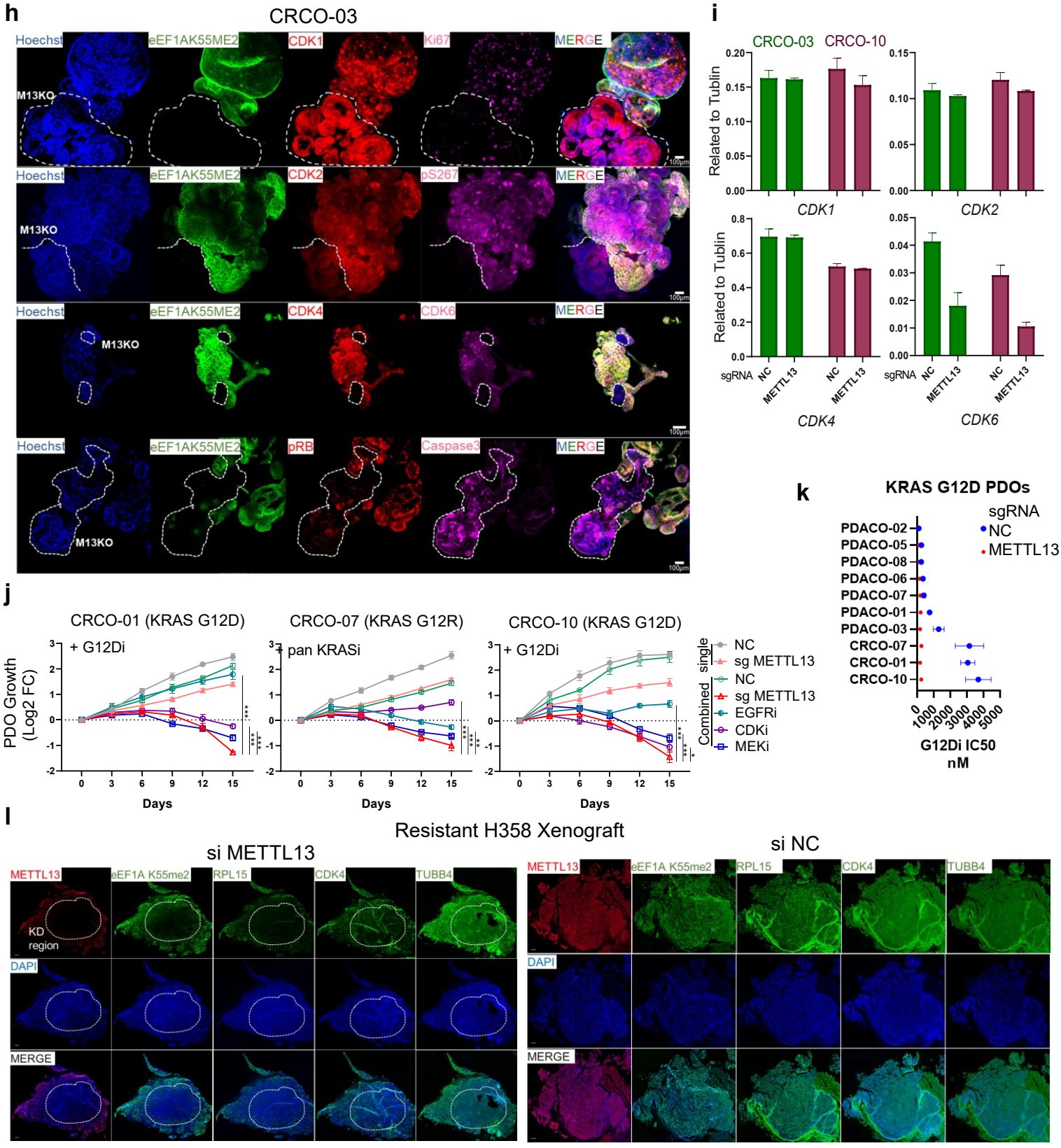
h
CRCO-03
Hoechst
eEF1AK55ME2
CDK1
Ki67
MERGE
M13KO
CDK2
pS267
CDK4
CDK6
pRB
Caspase3
i
CRCO-03
CRCO-10
Related to Tublin
CDK1
CDK2
CDK4
CDK6
sgRNA
NC
METTL13
j
CRCO-01 (KRAS G12D)
+ G12Di
CRCO-07 (KRAS G12R)
+ pan KRASi
CRCO-10 (KRAS G12D)
PDO Growth
(Log2 FC)
Days
single
Combined
NC
sg METTL13
EGFRi
CDKi
MEKi
k
KRAS G12D PDOs
sgRNA
NC
METTL13
PDACO-02
PDACO-05
PDACO-08
PDACO-06
PDACO-07
PDACO-01
PDACO-03
CRCO-07
CRCO-01
CRCO-10
G12Di IC50
nM
l
Resistant H358 Xenograft
si METTL13
si NC
METTL13
eEF1A K55me2
RPL15
CDK4
TUBB4
KD
region
DAPI
MERGE

Supplementary Fig. S5. a, IF analysis of EBFP, EGFP, pS267-METTL13 and ki67 in CRCO-03 under control and $KRAS^{G12D}$i treatment, related to Fig. 2e and 2J. pS267-METTL13 colocalizes with high CGA TE in proliferative cells. Scale bars: 20 µm. **b**, IF analysis of Hoechst, eEF1A K55me2 (left), METTL13 (right), pS267-METTL13 and Ki67 in CRCO-03 PDOs. Scale bars: 20 µm. eEF1A K55me2, METTL13, and pS267-METTL13 showed stronger signals in proliferative cells. **c**, Growth curves of CRC PDOs with RAS activation in the control and METTL13 KO conditions, related to Fig. 5b. **d**, IF analysis of the indicated proteins in RAS inactive PDOs (-02) in the control (NC) and METTL13 KO conditions. Scale bars: 20 µm. **e**, Quantification of proliferative cells in RAS inactive PDOs (-02 and -06) in the NC and METTL13 KO conditions. Each dot represented one organoid. Data are presented as mean ± SD, analyzed by paired t-test, n=10. **f**, Growth curves of CRCO-02 and -06 in the NC and METTL13 KO conditions. **g**, CGA frequency of CDK1, CDK2, CDK4, and CDK6 coding sequences. **h**, IF analysis of Hoechst, eEF1A K55me2, CDK1, CDK2, CDK4, pRB (red), Ki67, pS267-METTL13, CDK6 and cleaved caspase-3 (violet) in the co-cultured NC and METTL13 KO CRCO-03 PDOs. Scale bars: 100 µm. METTL13 KO organoids (marked by white dashed lines) showed loss of eEF1A K55me2 signal. **i**, RT-qPCR analysis of CDKs in CRCO-03 and -10 in the NC and METTL13 KO conditions. METTL13 KO did not affect mRNA level of CDK1/2/4. **j**, Proliferation assay of CRC PDOs treated with RAS inhibitors (G12Di: MRTX 1133, 1 µM; pan-KRASi: RMC-6236, 1 µM) combined with METTL13 KO, EGFRi (Oritinib, 1 µM), CDKi (Palbociclib, 1 µM), or MEKi (Trametinib, 0.5 µM). Data of c, f and j are presented as mean ± SD, analyzed by two-way ANOVA followed by Tukey's multiple comparisons test. **k**, Dose-response curves of MRTX 1133 in *KRAS*^{G12D}-mutant CRC and PDAC PDOs, related to Fig. 5h. Data are presented as mean ± SEM. **l**, IF analysis of the indicated proteins in acquired resistant H358-derived xenografts in the control (si-NC) and METTL13 KD conditions. METTL13 KD tumors (marked by white dashed lines) showed reduced levels of high-CGA proteins RPL15 and CDK4, but not TUBB4 (control), related to Fig. 5k. Scale bars: 100 µm. (*$P < 0.05$, **$P < 0.01$, ***$P < 0.001$).

Figure S6

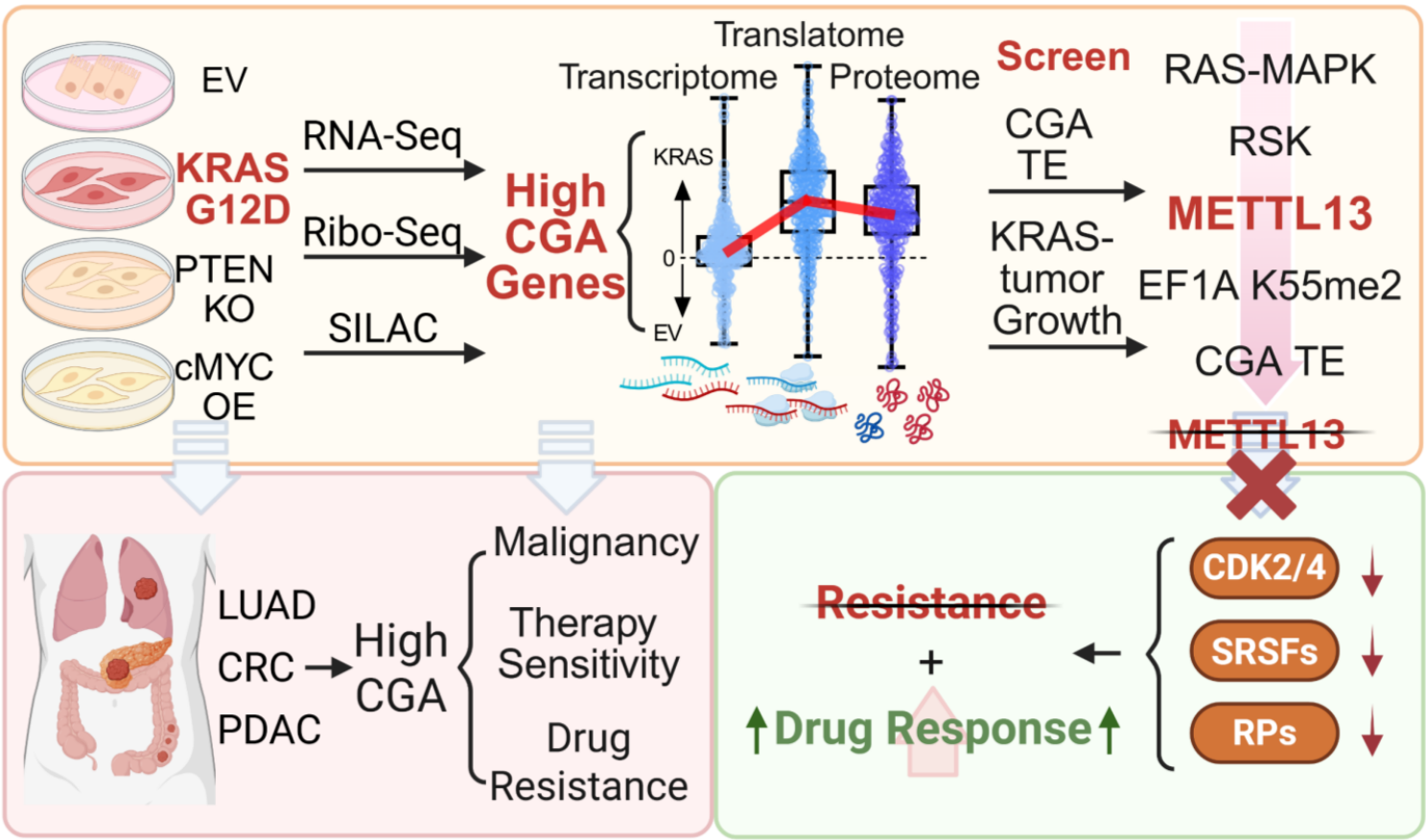
EV
KRAS G12D
PTEN KO
cMYC OE
RNA-Seq
Ribo-Seq
SILAC
High CGA Genes
Translatome
Transcriptome
Proteome
KRAS
0
EV
Screen
CGA TE
KRAS-tumor Growth
RAS-MAPK
RSK
METTL13
EF1A K55me2
CGA TE
METTL13
LUAD
CRC
PDAC
High CGA
Malignancy
Therapy Sensitivity
Drug Resistance
Resistance
+
Drug Response
CDK2/4
SRSFs
RPs

Supplementary Fig. S6 Proposed model of the METTL13–eEF1A K55me2–CGA axis in promoting tumor growth and drug resistance in RAS-activated tumors.